ISSN 1674-1056
http://cpb.iphy.ac.cn
http://iopscience.iop.org/cpb
中国物理 B
Chinese Physics
中国物理 Chinese Physics B

Digitally calibrated broadband gases absorption spectral measurements

Xinyi Chen(陈馨怡), Weipeng Zhang(张伟鹏), Haoyun Wei(尉昊赟), Yan Li(李岩)

Citation: Chin. Phys. B . 2019, 28(6): 060703. **doi:** 10.1088/1674-1056/28/6/060703
Journal homepage: http://cpb.iphy.ac.cn; http://iopscience.iop.org/cpb

What follows is a list of articles you may be interested in

Spectral distortion of dual-comb spectrometry due to repetition rate fluctuation

Hong-Lei Yang(杨宏雷), Hao-Yun Wei(尉昊赟), Yan Li(李岩)
Chin. Phys. B . 2016, 25(4): 044207. **doi:** 10.1088/1674-1056/25/4/044207

Joint transfer of time and frequency signals and multi-point synchronization via fiber network

Nan Cheng(程楠), Wei Chen(陈炜), Qin Liu(刘琴), Dan Xu(徐丹), Fei Yang(杨飞), You-Zhen Gui(桂有珍), Hai-Wen Cai(蔡海文)
Chin. Phys. B . 2016, 25(1): 014206. **doi:** 10.1088/1674-1056/25/1/014206

Optical coherence transfer over 50-km spooled fiber with frequency instability of 2×10^{-17} at 1 s

Ma Chao-Qun, Wu Li-Fei, Jiang Yan-Yi, Yu Hong-Fu, Bi Zhi-Yi, Ma Long-Sheng
Chin. Phys. B . 2015, 24(8): 084209. **doi:** 10.1088/1674-1056/24/8/084209

Non-contact angle measurement based on parallel multiplex laser feedback interferometry

Zhang Song, Tan Yi-Dong, Zhang Shu-Lian
Chin. Phys. B . 2014, 23(11): 114202. **doi:** 10.1088/1674-1056/23/11/114202

A sensitive method of determining optic axis azimuth based on laser feedback

Wu Yun, Zhang Peng, Chen Wen-Xue, Tan Yi-Dong
Chin. Phys. B . 2013, 22(12): 124205. **doi:** 10.1088/1674-1056/22/12/124205

Digitally calibrated broadband dual-comb gases absorption spectral measurements*

Xinyi Chen(陈馨怡), Weipeng Zhang(张伟鹏), Haoyun Wei(尉昊赟)†, and Yan Li(李岩)

State Key Laboratory of Precision Measurement Technology & Instruments, Department of Precision Instrument, Tsinghua University, Beijing 100084, *China*

(Received 28 January 2019; revised manuscript received 1 April 2019; published online 8 May 2019)

From the perspective of error compensation in the sampling process, a digital calibration algorithm was studied for the processing of spectral data in dual-comb spectroscopy. In this algorithm, dynamic adaptation to phase fluctuations maintained constant measurement results of spectral line positions and intensities. A mode-resolved broadband absorption spectrum was obtained over the full-spectral range of the comb with a Hertz linewidth of radio frequency comb mode. The measured spectrum spanned over 10 THz, which covered the multiplexed absorption regions of mixed gases, such as CO_2 and N_2O. The calibrated interferograms were also capable of direct coherent averaging in the time domain. The transmittance obtained deviated from the theoretical calculation by no more than 2% in the whole spectral span.

Keywords: dual-comb spectroscopy, digital calibration

PACS: 07.57.Ty, 42.62.Eh, 29.30.–h **DOI:** 10.1088/1674-1056/28/6/060703

1. Introduction

The types and concentrations of gases have been the focus of environmental monitoring, global climate change,[1] human respiratory health,[2] *etc*. Absorption spectral measurement is an effective method for these demands and it has been implemented on various configurations, such as Fourier transform spectrometers and laser spectrometers.[3–12] Among these methods, the dual-comb spectrometer has attracted much attention due to its potential for short acquisition time and broad spectral bandwidth, which could cover multiplexed molecular absorption regions.[13–20] However, achieving a high spectral resolution posts critical requirements for the frequency stability and mutual coherence in the dual-comb system. The commonly used comb configuration, such as using a Rb atomic clock as a radio frequency (RF) reference, is insufficient to obtain a mode-resolved spectrum due to the large phase fluctuations of the two parameters of combs; namely, the repetition rate $f_{\rm rep}$ and the carrier envelope offset $f_{\rm ceo}$. Moreover, since the two combs are locked independently, their phase is irrelevant, which causes dramatic distortions in the interferograms (IGMs) and obstacles the possibility to achieve higher resolution and signal-to-noise ratio (SNR).

The coherence between two combs can be recovered by stabilizing the combs against two state-of-the-art cavity-stabilized continuous-wave (CW) lasers, which have hertz-level line-widths and could result in the multi-heterodyne signals over several seconds.[21–23] Unfortunately, this stabilization scheme requires demanded experimental conditions, including the phase-locking electronics with high dynamic bandwidth, and thus limits its applicable range. Another feasible method is to use the adaptive resampling technique,[24] which was implemented by introducing additional lasers as an intermediary. This technique enables reconstruction of a linear time axis for the unstable combs, either by hardware triggered acquisition[24–27] or software compensation.[28–30] Continuous real-time averaging of IGMs up to days in length[27,30] has been demonstrated, which was implemented with a field-programmable gate array (FPGA) development board. Measurements with high SNR and resolution were shown, confirming that the dual-comb interferometer can maintain excellent working performance without tight locking.

In this work, we obtain a mode-resolved mixed gas absorption spectrum over a broad-spectral range by a digital calibration algorithm. The detection of long-path gases absorption is performed under laboratory conditions and is completed by digital calibration without using the electrical phase lock loops to tightly lock the combs. Two free-running CW lasers have been used to provide the reference information about the unsynchronized phase between the two combs, assisting the time domain averaging of the IGMs and resulting in the clear spectral lines. In the following sections, we will introduce the principle, illustrate the experimental setup, and discuss the validity of the algorithm by our measurement results.

2. Theory

The phase fluctuations of the difference of repetition rate Δf_r between the two combs (Comb1, Comb2) distort the linearity of the time axis of the multi-heterodyne interference signals. Meanwhile, the fluctuations of the difference of carrier

*Project supported by the National Natural Science Foundation of China (Grant No. 61775114).

†Corresponding author. E-mail: luckiwei@mail.tsinghua.edu.cn

© 2019 Chinese Physical Society and IOP Publishing Ltd

envelope offset $\Delta f_{\rm ceo}$ lead to unstable phase in the time domain. Fortunately, these phase fluctuations can be extracted from the linear combination of the transition beat signals between two CW lasers (CW1, CW2) and two combs, as shown in Fig. 1(a).

The Δphase1 and the Δphase2 in Fig. 1(a) are the phase changes of the beats between the same CW laser and two combs. The essential function of the CW lasers is to obtain the beat of one dual-comb teeth pair near the frequency of the CW lasers. Any fluctuations of the CW laser are removed when beat1 is combined with beat2 (or beat3 with beat4). Ideally, Δphase1 and Δphase2 should increase linearly. The deviations from linear values represent the effects of the incoherent phase fluctuations between the two combs. This contains the information about the phase fluctuations of $\Delta f_{\rm r}$ and $\Delta f_{\rm ceo}$, as shown in Eq. (1), where $f_{\rm rep1}$ and $f_{\rm rep2}$ are the repetition rates of Comb1 and Comb2, and n_1 and n_2 mean the numbers of the teeth of Comb1 and Comb2 adjacent to CW1, respectively. $f_{\Delta\rm phase1}$, $f_{\rm beat1}$, and $f_{\rm beat2}$ represent the frequencies corresponding to their subscripts respectively. Subsequent variables have a similar form, such as $f_{\Delta\rm phase2}$, $f_{\rm beat3}$, $f_{\rm beat4}$, and $f_{\Delta\rm phase}$. When $f_{\rm rep1}$ and $f_{\rm rep2}$ are integer multiples of $\Delta f_{\rm r}$, the item $(n_2-n_1)*f_{\rm rep2}$ can be merged into the term containing $\Delta f_{\rm r}$. Then the $f_{\Delta\rm phase1}$ and the $f_{\Delta\rm phase2}$ can be written as the last expression shown in Eqs. (1) and (2), where M_1 equals $n_1-(n_2-n_1)*(f_{\rm rep2}/\Delta f_{\rm r})$. Otherwise, the initial phase of the IGM could be slightly influenced by the fluctuation of $f_{\rm rep2}$. The value of (n_2-n_1), however, is usually a one-digit small value, such as 1, 2, 3, while n_1 is on the order of hundreds of thousands. Thus, the influence led by this item could be reasonably neglected. Similarly, the $f_{\Delta\rm phase2}$ can be expressed as Eq. (2), where m_1 and m_2 denote the number of the teeth of Comb1 and Comb2 adjacent to CW2, and M_2 equals $m_1-(m_2-m_1)*(f_{\rm rep2}/\Delta f_{\rm r})$.

$$\begin{aligned} f_{\Delta\rm phase1} &= f_{\rm beat1}-f_{\rm beat2}=\Delta f_{\rm ceo}+n_1*\Delta f_{\rm r}-(n_2-n_1)f_{\rm rep2} \\ &= \Delta f_{\rm ceo}+M_1*\Delta f_{\rm r}, \qquad (1) \\ f_{\Delta\rm phase2} &= f_{\rm beat3}-f_{\rm beat4}=\Delta f_{\rm ceo}+m_1*\Delta f_{\rm r}-(m_2-m_1)f_{\rm rep2} \\ &= \Delta f_{\rm ceo}+M_2*\Delta f_{\rm r}, \qquad (2) \\ f_{\Delta\rm phase} &= f_{\Delta\rm phase1}-f_{\Delta\rm phase2}=(m_1-n_1)*\Delta f_{\rm r}, \qquad (3) \\ {\rm comb}_{\rm RF} &= \Delta f_{\rm ceo}+\sum_n n*\Delta f_{\rm r}. \qquad (4) \end{aligned}$$

The Δphase is the difference between Δphase1 and Δphase2. Its deviations from the linear values only contain the phase fluctuations of $\Delta f_{\rm r}$, as shown in Eq. (3). In our setup, the value of (m_1-m_2) equals that of (n_1-n_2), because of the appropriate optical measurement bandwidth determined by the selected $\Delta f_{\rm r}$, and thus, equation (3) is workable. Based on these expressions of Δphase1, Δphase2, and Δphase, we can extract the phase fluctuations of the two variables ($\Delta f_{\rm r}$ and $\Delta f_{\rm ceo}$) separately.

The RF-comb generated by the interference of two combs can be expressed as the linear combination of $\Delta f_{\rm r}$ and $\Delta f_{\rm ceo}$, as shown in Eq. (4), where n is determined by the measurement bandwidth and $\Delta f_{\rm r}$. Therefore, the acquired phase fluctuations of $\Delta f_{\rm r}$ and $\Delta f_{\rm ceo}$ could effectively calibrate the dual-comb interference signals.

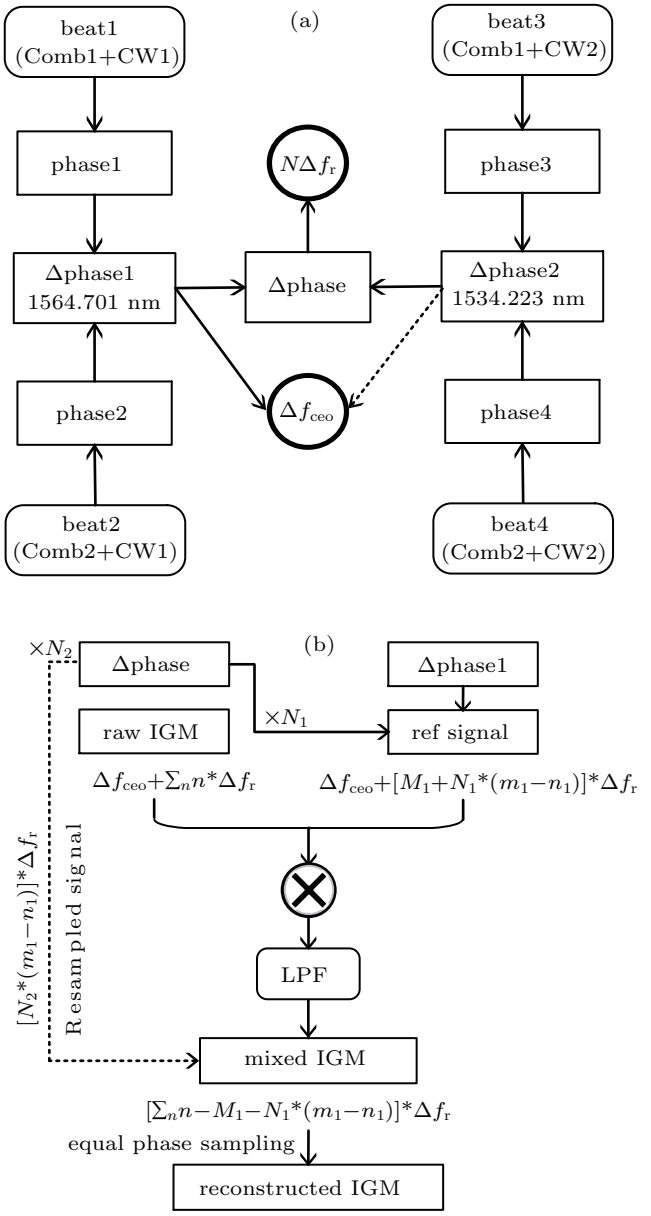


Fig. 1. (a) Principle of digital calibration. The dotted line explains that Δphase2 contains the information about the phase fluctuations of $\Delta f_{\rm ceo}$ but is not used for extraction. (b) Process of digital calibration. LPF: lowpass filter. N_1: the coefficient of Δphase in the signal used for mixing aim to avoid frequency aliasing. N_2: the coefficient of Δphase in the signal used for resampling.

The process of obtaining a spectrum mainly consists of two major parts, which are depicted in Fig. 1(b). First, the fluctuations of the $\Delta f_{\rm ceo}$ are mixed with the IGMs in order to calibrate the unstable phases. To avoid frequency aliasing, the Δphase and the Δphase1 are used simultaneously. Specifically, we use a linear combination of $f_{\Delta\rm phase}$ and $f_{\Delta\rm phase1}$ for the mixing process, which lay outside the frequency range of the orig-

inal IGMs. For the purpose of eliminating the influence of the phase fluctuations of Δf_{ceo}, the signals used for combining can contain only a single f_{ceo}, which is consistent with the form of the RF comb. Second, equiphase resampling is performed on the mixed IGMs, using the fluctuations of the Δf_{r}. What needs to be explained is the selection of N_2, the coefficient of Δphase as described in Fig. 1(b). The basic principle is to satisfy the sampling law. The frequency of the interference signal is on the order of 10 MHz, and the sampling frequency we choose can guarantee the lossless recovery of the interference signal. After these two steps, the reconstructed IGMs have good repeatability, which permits averaging in the time domain and provides measurements result with higher resolutions than that of a single measurement.

3. Experimental setup

Figure 2 illustrates the schematic of our dual-comb spectrometer (DCS). We used this system for spectral measurements with the digital calibration algorithm mentioned previously. Two free-running diode lasers (Redfern Integrated Optics, 1564.701 nm, 1534.223 nm) are used as the CW reference lasers, which locate within the measurement bandwidth. Since the fluctuations of the CW lasers are removed in the process of algorithm subtraction, the greater influence on the measurement results is the line width of the lasers. The lasers that we used have a nominal linewidth less than 2 kHz, which effectively ensures the extraction of the reference information. In addition, we have added slow loop feedback to the CW lasers to ensure the stability of the system since the frequency of the beat signals of the combs and the CW lasers may be jittered, which may exceed the operating range of filters, amplifiers, *etc*. Two optical frequency combs (Menlo systems, FC-1500) are used as the light sources, which have repetition rates of about 250 MHz. This system can work with the free-running combs except that the positions of the absorption lines may drift due to the changes in Δf_{r}. In this case, it is necessary to detect f_{r}, which will be used to determine the coordinates. We suggest that f_{r} of the two combs can be locked to highly stabled frequency standards, such as rubidium clock. Our algorithm is used to compensate the jitters of f_{ceo}, the unsynchronized phase fluctuations between the two combs. This method is easy to implement and guarantees high quality results. We have used the system to perform multiple measurements at different times and the spectral curves always maintain a stable and sufficient signal-to-noise ratio after processing by our algorithm.

Fiber Bragg gratings (FBGs) are used as an optical filter, with a bandwidth of about only 0.2 nm and a high reflectance greater than 99%. We cascade two FBGs instead of putting them in two branches, effectively improving the efficiency of optical power and avoiding the limitation about the optical delay range mentioned in the previous literature.[28] Four fiber polarization controllers (PCs) are used to control the polarization of the light from the CW lasers to enhance the SNR of the beat signals between the lasers and the combs. If the output power of the light source is sufficient to ensure that the signal has an ideal SNR, then it is not necessary to use these polarizing devices. Balanced detection is used to maximize the dynamic range available for the heterodyne signal by suppressing the strong homodyne signal from the individual channels. At the same time, the balanced detectors (New Focus, 1837, 300 MHz) achieve simultaneous detection of the two optical signals, reducing the number of required acquisition channels and attenuating the effects of power fluctuations of the CW laser. The signals are all recorded by the high-speed digitizer (National Instruments, NI 5761, 4 CHs, 14 bits, 250 MS/s). An on-board random-access memory (RAM) is used as a large capacity storage buffer, allowing high throughput acquisition and processing. The acquisition time can reach 1.6 s, and recording a single IGM requires 3.47 ms (Δf_{r} equals 288 Hz), which means 460 consecutive IGMs can be averaged within a single acquisition.

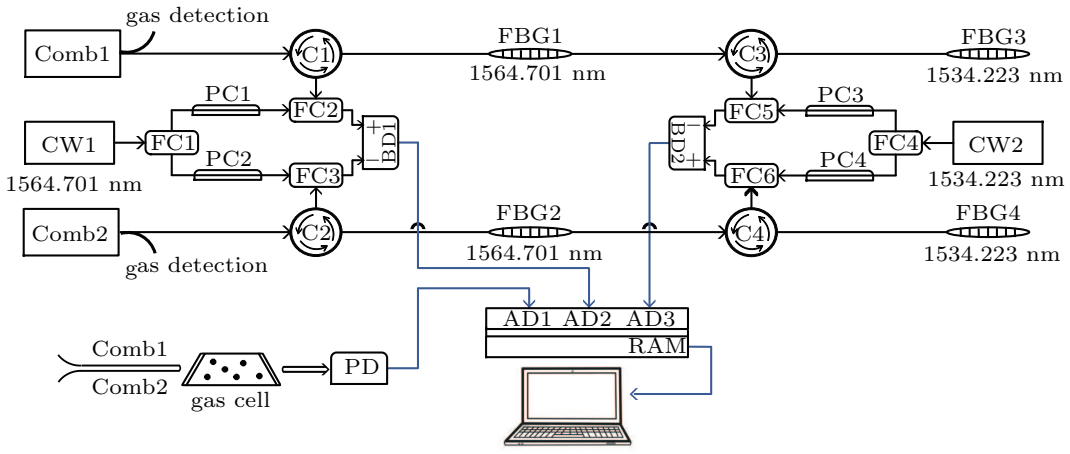


Fig. 2. Schematic diagram of digitally calibrated DCS. Comb1 and Comb2: optical frequency comb. CW1 and CW2: continuous wave laser. C1–C4: fiber circulator. FBG1–FBG4: fiber Bragg grating. FC1–FC6: fiber coupler. PC1–PC4: fiber polarization controller. BD1 and BD2: balance detector. PD: Photodetector. AD1–AD3: analog to digital converter. RAM: random-access memory. Black solid line: fiber. Blue solid line: cable.

In this paper, we have measured a mixture of two gases, CO_2 and N_2O, considering their significant contribution to the greenhouse effect. Due to their weak absorption in the near infrared region, a kilometre-scale absorption length, such as open-path measurements, is always needed to acquire meaningful absorption features for quantitative analysis. This is difficult for laboratory conditions, even with the help of multi-pass gas cell. To demonstrate nearly equivalent absorption intensity measurements for open path applications, we fill a gas cell (685-cm multi-path gas cell) with a total pressure of 1 atm (1 atm = 1.01325×10^5 Pa) and a mixing ratio of 60:40 (CO_2:N_2O). This mixing ratio is not necessary. We choose this ratio mainly to prove that the system does have the high-precision broadband measurement capabilities. Since the absorption of N_2O is very strong in this range (line strength is on the order of 10^{23}, even higher than CO_2), we choose this ratio to enable that the absorption lines of both gases can be clearly seen in the spectral curve.

4. Results

4.1. Results of the digital calibration

Figure 3 shows the transmission spectra retrieved from the full length original and calibrated IGMs. Here, eight single consecutive spectra and an averaged one of 460 spectra in a zoomed-in window of the full spectral span are displayed for comparison. It is obvious that the uncalibrated spectrum in Fig. 3(a) is poorly distorted owing to the phase fluctuations of Δf_r and Δf_{ceo}, and the absorption features are nearly eliminated in the averaged one. This means that direct extraction of spectral information is almost impossible by using the current dual-comb source. In contrast, the calibrated spectrum, as shown in Fig. 3(b), is able to reproduce the spectral line positions and absorption signal intensities. Moreover, the averaged spectrum exhibits a higher SNR because the random noise is suppressed. This comparison confirms the necessity of recovering the mutual coherence between the two combs and the feasibility of the calibration technique in our experiment.

To further exploit the potential of the adaptive algorithm for mutual coherent recovering, the spectra of the beat signal between one dual-comb teeth pair are illustrated in Fig. 4 with different Fourier transformed lengths. The spectra of the uncalibrated beat are severely distorted and have a width of about 0.25 MHz, even though longer lengths of data have been used as shown in Fig. 4(a). This width has far exceeded the down-converted comb interval in RF, which should equal 288 Hz in our experiment, and will seriously blur the absorption features. Fortunately, after calibration, all the full widths at half maximum (FWHMs) corresponding to each data length reveal significant improvement. The FWHMs are gradually narrowed by an order of magnitude as shown in the four curves in Fig. 4(b). In the red curve, 1-s length of data is used. The FWHM is only about $1/2\times10^5$ of that uncalibrated one and reaches the corresponding Fourier transform limitation. It is worth noting that the trend of improvement has been maintained with the increase of the acquisition time.

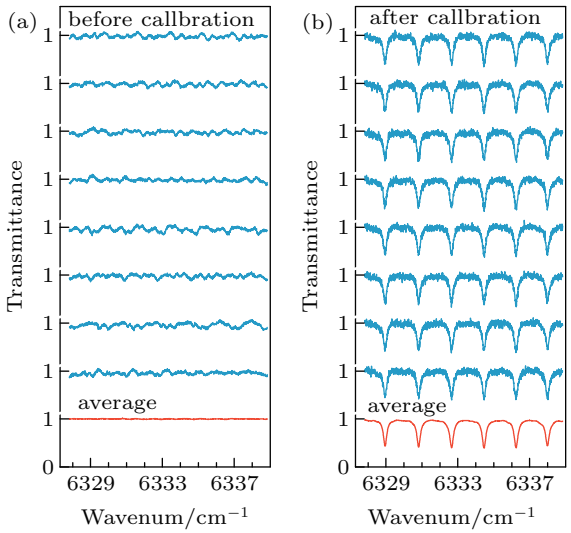


Fig. 3. A comparison of the transmission spectra retrieved from the full length original and calibrated IGMs in an 11-cm^{-1} zoomed-in portion. (a) Eight single consecutive spectra (in blue) and an averaged one of 460 spectra (in red) before digital calibration. (b) Calibrated spectra and other conditions are the same as those in panel (a).

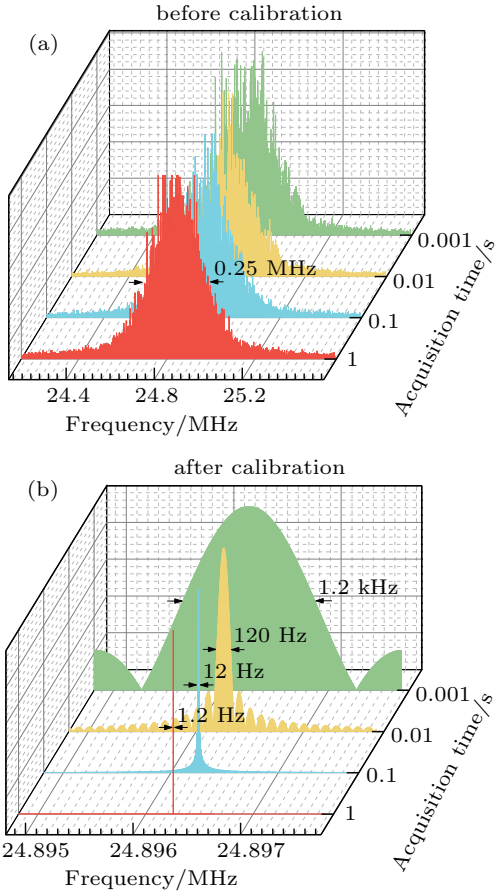


Fig. 4. The spectra of the beat signal between one dual-comb teeth pair at different acquisition times. Different colors represent different times. (a) Before calibration. (b) After calibration.

In addition, the capability of time-domain interferometric co-adding is verified as shown in Fig. 5(a) by applying the calibration algorithm. Single IGM after calibration and an averaged one of 460 consecutive calibrated IGMs are shown together. The bursts and the interference data, which are away from the center, are shown in the zoomed parts of Fig. 5(a). The bursts of the averaged one and the single one have almost the same shapes, indicating the high consistency of the calibrated IGMs. Moreover, the noise shown in the zoomed-in part, which is on the right-hand side, is significantly suppressed, suggesting that the digital calibration permits efficient averaging as a result of the elimination of the above-mentioned phase fluctuations. Finally, the IGMs are normalized to their peak intensities and the SNR in the time domain is defined as the reverse of standard deviation of the data away from the bursts (the zoomed part) in this paper. The SNR scales as the square root of the numbers used for co-adding as plotted in Fig. 5(b). According to the trend of the fitted curve, the SNR experiences no deviation from linearity when the averaged number increases, implying that the coherence between the two combs is well maintained during the measurement by our calibration. The co-added IGM has an SNR of 36012 with a measurement time of 1 s, while the directly added IGM without calibration has an SNR of only 1067. Furthermore, no optical filters are used during the measurements, and thus, the full spectral range of the combs could be measured without any switching of optical filters. All these results proof the feasibility of high-quality spectral measurements.

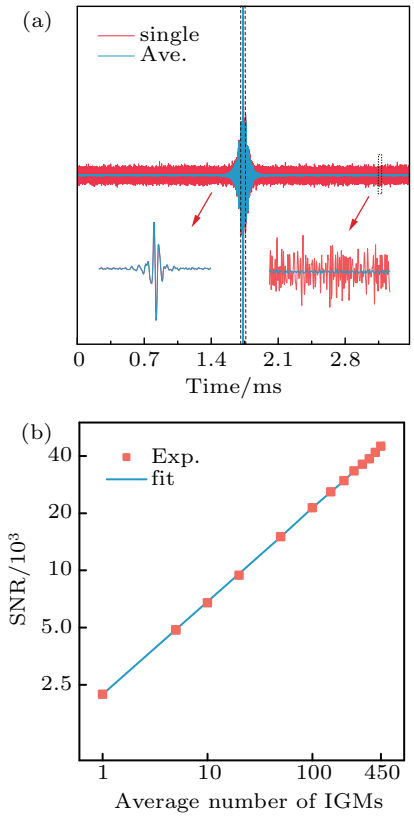


Fig. 5. (a) IGMs in the time domain. Single IGM after calibration (in red) and an averaged one of 460 consecutive calibrated IGMs (in blue). The bursts (left) and the interference data away from the center (right) are shown in the zoomed parts. (b) The time domain SNR of the calibrated IGMs with different co-adding numbers.

4.2. Results of the spectral measurements

A mode-resolved spectrum is obtained since the direct Fourier transform is performed on the calibrated continuous long-term interference data. The measurement time is 1.6 s, which is limited by the memory depth of the on-board RAM. The spectrum spans over 10 THz, which covers numerous complex and dense absorption lines of CO_2 and N_2O, as shown in Fig. 6. Current spectral bandwidth is only limited by the output of the dual-comb source and can be extended to longer wavelengths as explored in previous work.[31–34] Figure 6(e) shows the full span of the spectrum, which contains more than 40000 comb modes. In order to observe the equidistance comb modes clearly, we show two spectral regions on different scales. Figure 6(c) shows a mode-resolved absorption line of CO_2 and four equally spaced comb modes at the lowest point of this absorption line are shown in Fig. 6(a). The mode interval is 288 Hz in the RF domain, corresponding to 250 MHz in the optical frequency (OF) domain. Figure 6(d) shows the equal-intensity comb modes in the region that is absent of absorption. The middle-most mode is shown in Fig. 6(b), which has an FWHM of 0.75 Hz in the RF domain corresponding to 651 kHz in the OF domain. Finally, the dense absorption area of N_2O is shown in Fig. 6(f) with an enlarged view, expressing the results of the mixed gas measurements. The triangular gap is determined by the absorption characteristics of N_2O. High-resolution transmission molecular absorption (HITRAN) database shows the same result under the same experimental conditions. According to these results, the instrumental linewidth is 0.75 Hz in the RF domain and the corresponding resolution in OF domain has been much smaller than the repetition rate of the combs. The well-resolved comb modes indicate that the resolution of our system is sufficient for the spectral measurements of gases at normal pressures and temperatures.

The transmittance is obtained by applying the baseline correction. Unlike in the trace gas measurements, where the shape of the baseline remains relatively intact, the baseline is difficult to determine in our experiments, due to the strong gas absorption. So we add the baseline as an additional parameter when performing the fitting of the spectrum, where the transmittance and the baseline are obtained simultaneously. The results are in good agreement with the theoretical transmission curve calculated using the HITRAN database, and the maximum deviation within the full spectral region does not exceed 2%. We compare the partial experimental transmittance with

the calculated transmission curve at different scales in Fig. 6. The full branch lines of the $3\nu_1$ ro-vibration of CO_2 molecule are shown in Fig. 6(a). The fine absorption lines on the left are the contribution of N_2O. The P14e line of in this ro-vibration band is shown in Fig. 6(b). The circled area in Fig. 6(b) contains the information of a weak absorption line of another ro-vibration line ($3\nu_1+\nu_2+\nu_3$ to $\nu_2+\nu_3$, P24f). The line intensity at this frequency (S, 4.831×10^{-25} cm/mol) is only about one percent of that at the adjacent strong absorption line (S, 1.619×10^{-23} cm/mol), revealing the sufficient SNR for measurements of weak absorptions. These clear transmission lines proof that this spectrometer setup and our digital calibration algorithm are capable of broadband mixed gas detection and suggest the feasibility of gases monitoring.

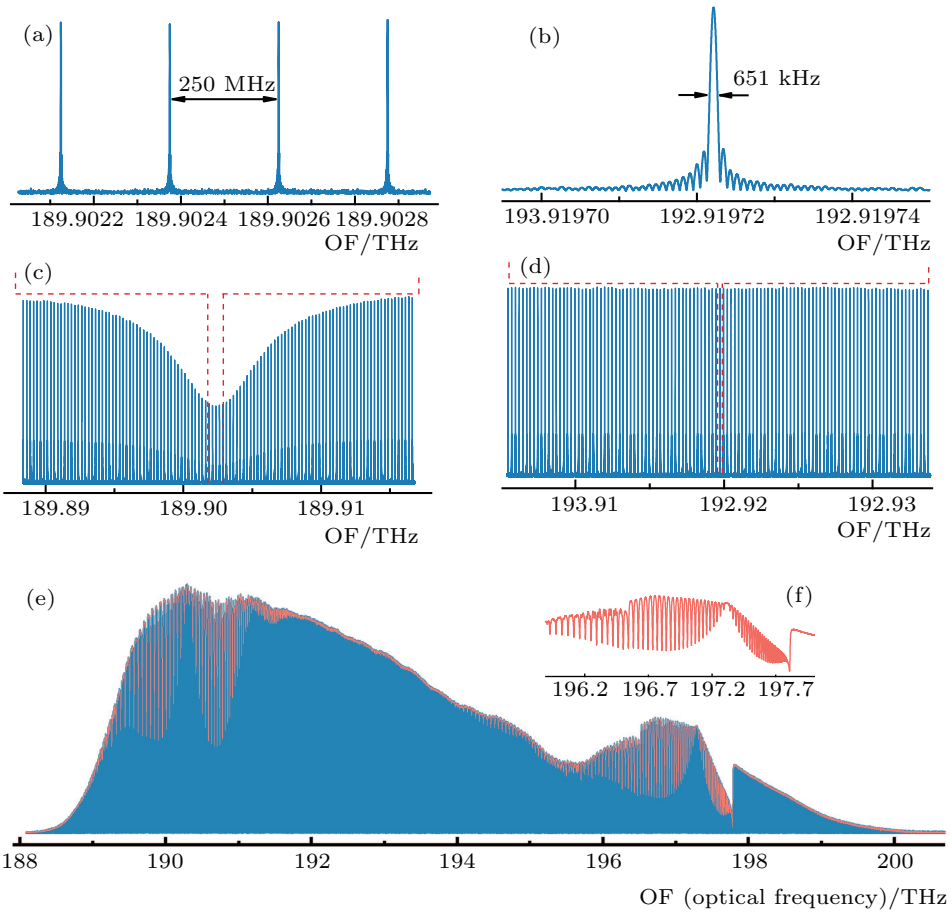


Fig. 6. Mode-resolved broadband mixed gas absorption spectra. (a)–(d) Two different spectral regions, with and without absorption, are displayed at different scales for better demonstrating the well-resolved comb lines. (e) Calibrated spectrum spanning over 10 THz. (f) An enlarged view of the dense absorption area of N_2O.

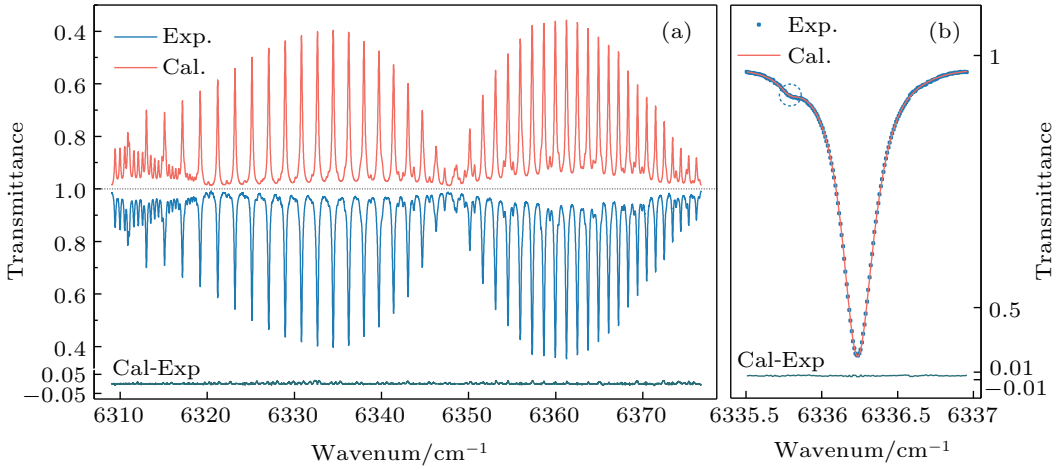


Fig. 7. Partial transmission spectra of the mixed gas. The experimental transmittance is compared with the transmission curve calculated from the parameters provided by the HITRAN database, together with the residuals. (a) The full branch lines of the $3\nu_1$ ro-vibration of CO_2 molecule. Part of the absorption of N_2O is contained in the leftmost area. (b) The P14e transition line of the $3\nu_1$ ro-vibration of CO_2 molecule. The circled area contains the weak absorption information of the P24f line of $3\nu_1+\nu_2+\nu_3$ to $\nu_2+\nu_3$ ro-vibration.

5. Conclusion

The feasibility of our digital calibration algorithm is adequately verified in both the time domain and the frequency domain. The algorithm effectively suppresses the influence of the unsynchronized phase in the dual-comb system that originates from the phase fluctuations of Δf_{r} and Δf_{ceo}. Therefore, a mode-resolved mixed gas absorption spectrum was obtained, which spans the full spectral range of the combs. The mutual coherence of the dual-comb system is well recovered over the time of measurements, which suggests high-quality multi-heterodyne spectroscopy from the time domain co-adding. The sufficient resolution shown in the experimental spectra confirms the suitability of our system for the mixed gas measurements. A potential higher SNR over a longer average time can serve gas monitoring with a strict precision requirement. According to these results, the application range of the dual-comb interferometer can be expected to have a further extension without tight locking.

References

[1] Pearce W, Holmberg K, Hellsten I and Nerlich B 2014 *PLoS One* **9** e94785

[2] Lelieveld J, Evans J S, Fnais M, Giannadaki D and Pozzer A 2015 *Nature* **525** 367

[3] Hodgkinson J and Tatam R P 2013 *Meas. Sci. Technol.* **24** 012004

[4] Fiorani L, Santoro S, Parracino S, Nuvoli M, Minopoli C and Aiuppa A 2015 *Opt. Lett.* **40** 1034

[5] Frankenberg C, Meirink J F, van Weele M, Platt U and Wagner T 2005 *Science* **308** 1010

[6] Rairoux P, Schillinger H, Niedermeier S, Rodriguez M, Ronneberger F, Sauerbrey R, Stein B, Waite D, Wedekind C, Wille H, Woste L and Ziener C 2000 *Appl. Phys. B: Lasers Opt.* **71** 573

[7] Fawcett B L, Parkes A M, Shallcross D E and Orr-Ewing A J 2002 *Phys. Chem. Chem. Phys.* **4** 5960

[8] Humphries S D, Nehrir A R, Keith C J, Repasky K S, Dobeck L M, Carlsten J L and Spangler L H 2008 *Appl. Opt.* **47** 548

[9] Stephan C, Alpers M, Millet B, Ehret G, Flamant P and Deniel C 2011 *Proc. SPIE* 8159 *Lidar Remote Sensing for Environmental Monitoring XII,* 815908 (Singh U N ed.)

[10] Wunch D, Toon G C, Blavier J F L, Washenfelder R A, Notholt J, Connor B J, Griffith D W T, Sherlock V and Wennberg P O 2011 *Philos. Trans. R. Soc. London Ser. A* **369** 2087

[11] Ramanathan A, Mao J, Allan G R, Riris H, Weaver C J, Hasselbrack W E, Browell E V and Abshire J B 2013 *Appl. Phys. Lett.* **103** 214102

[12] Khorsandi A, Shabani Z, Ranjbar M and Salati S A H 2012 *Chin. Phys. B* **21** 064213

[13] Rieker G B, Giorgetta F R, Swann W C, Kofler J, Zolot A M, Sinclair L C, Baumann E, Cromer C, Petron G, Sweeney C, Tans P P, Coddington I and Newbury N R 2014 *Optica* **1** 290

[14] Baumann E, Giorgetta F R, Rieker G B, Sinclair L C, Coddington I, Swann W C and Newbury N R 2015 *Advanced Solid State Lasers*, October 4–9, 2015, Berlin, Germany, p. ATh1A.5

[15] Schroeder P J, Wright R J, Coburn S, Sodergren B, Cossel K C, Droste S, Truong G W, Baumann E, Giorgetta F R, Coddington I, Newbury N R and Rieker G B 2017 *Proc. Combust. Inst.* **36** 4565

[16] Coddington I, Newbury N and Swann W 2016 *Optica* **3** 414

[17] Schiller S 2002 *Opt. Lett.* **27** 766

[18] Keilmann F, Gohle C and Holzwarth R 2004 *Opt. Lett.* **29** 1542

[19] Schliesser A, Brehm M, Keilmann F and van der Weide D W 2005 *Opt. Express* **13** 9029

[20] Zhang W P, Yang H L, Chen X Y, Wei H Y and Li Y 2018 *Acta Phys. Sin.* **67** 090701 (in Chinese)

[21] Coddington I, Swann W C and Newbury N R 2008 *Phys. Rev. Lett.* **100** 013902

[22] Coddington I, Swann W C and Newbury N R 2009 *Opt. Lett.* **34** 2153

[23] Jacquet P, Mandon J, Bernhardt B, Holzwarth R, Guelachvili G, Hänsch T W and Picqué N *Advances in Imaging* O S A Technical Digest (C D) (Optical Society of America 2009), p. FMB2

[24] Ideguchi T, Poisson A, Guelachvili G, Picqué N and Hänsch T W 2014 *Nat. Commun.* **5** 3375

[25] Ideguchi T, Poisson A, Guelachvili G, Hänsch T W and Picqué N 2012 *Opt. Lett.* **37** 4847

[26] Poisson A, Ideguchi T, Guelachvili G, Picqué N and Hänsch T W 2012 *Conference on Lasers and Electro-Optics*, May 6–11, 2012, San Jose, USA, p. CW1J.1

[27] Shen X, Yan M, Hao Q, Yang K and Zeng H 2018 *IEEE Photon. J.* **10** 1503309

[28] Giaccari P, Deschenes J D, Saucier P, Genest J and Tremblay P 2008 *Opt. Express* **16** 4347

[29] Deschenes J D, Giaccari P and Genest J 2010 *Opt. Express* **18** 23358

[30] Roy J, Deschenes J D, Potvin S and Genest J 2012 *Opt. Express* **20** 21932

[31] Yasui T, Saneyoshi E and Araki T 2005 *Appl. Phys. Lett.* **87** 061101

[32] Brehm M, Schliesser A and Keilmann F 2006 *Opt. Express* **14** 11222

[33] Yasui T, Kabetani Y, Saneyoshi E, Yokoyama S and Araki T 2006 *Appl. Phys. Lett.* **88** 241104

[34] Bartels A, Cerna R, Kistner C, Thoma A, Hudert F, Janke C and Dekorsy T 2007 *Rev. Sci. Instrum.* **78** 035107